Conformal transformation applied to plasmonics beyond the quasistatic limit

Alexandre Aubry, Dang Yuan Lei, Stefan A. Maier, and J. B. Pendry
The Blackett Laboratory, Department of Physics, Imperial College London, London SW7 2AZ, United Kingdom
(Received 28 July 2010; published 9 November 2010)

A general strategy has been proposed recently to design and study analytically plasmonic devices, such as kissing nanowires, which show unprecedented broadband and nanofocusing properties. These nanostructures result from a conformal transformation applied to infinite plasmonic systems. The conformal transformation tool is powerful since the whole problem is solved in the original frame under the quasistatic approximation. However, this strategy is quite restrictive in perspective of applications since it can only apply to nanostructures of a few tens of nanometers (typically 20 nm). In this study, we extend the range of validity of this approach by taking into account radiation damping. The radiative losses are shown to map directly onto the power dissipated by a fictive absorbing particle in the original frame. Whereas only the surface plasmon mode was considered in previous studies, here lossy surface waves are also taken into account. Their counterpart in the transformed frame is shown to contribute predominantly to the radiative losses. The radiative reaction is then taken into account to predict the optical response of the nanostructure beyond the quasistatic limit. Radiative losses are shown to limit the light harvesting process but improve its broadband feature. The field enhancement induced by the nanostructure decreases with the structure dimension but remains significant ($\sim 10^3$) over a major part of the near-infrared and visible spectra. Our analytical model is compared to numerical simulations and a quantitative agreement is found for dimension up to 200 nm.

DOI: 10.1103/PhysRevB.82.205109 PACS number(s): 78.67.Bf, 73.20.Mf

I. INTRODUCTION

Transformation optics has drawn a considerable attention for the last 5 years. The paths of electromagnetic waves can be controlled by devising a material whose constitutive parameters should vary spatially in a way prescribed by coordinate transformations. Following the seminal works of Leonhardt[1] and Pendry *et al.*,[2] various applications have been proposed and implemented experimentally, among which is the electromagnetic cloak.[3–8] This strategy has been recently extended to plasmonics.[9–11] By devising the optical parameters of the dielectric placed on top of a metal surface, one can design plasmonic devices capable of different functionalities such as beam shifting or cloaking. At the same time, an original approach, based on conformal transformation, has been proposed to design and study analytically broadband plasmonic devices acting as strong field concentrators.[12–15] The idea is the following: start with an infinite plasmonic structure that naturally shows a broadband spectrum; then, by applying a conformal transformation to this system, a finite plasmonic structure is obtained. This one shows considerable nanofocusing properties over a broadband spectrum. This conformal transformation approach is powerful since the material permittivity is conserved. Hence, it does not require the delicate design of a metamaterial with a spatial variation in its constitutive parameters. However, this strategy is only valid in the quasistatic limit. Its range of application is thus restricted to plasmonic devices whose dimension D is at least one order of magnitude smaller than the wavelength (typically $D<20$ nm in the optical regime[12–14]).

In this study, we show how to extend this conformal transformation approach to devices of much larger dimensions. Rigorously, this should be done by considering the magnetic component in addition to the electric field. However, this would be particularly tedious and untractable analytically since the permeability is not conserved and should vary spatially as $1/r^2$ in the original frame.[16] In this paper, we propose an alternative and finer route based on energy arguments. It consists in extending the electrostatic results by taking into account radiation damping. For simplicity but without loss of generality, we will consider the example of the transformation described in Fig. 1, already studied in the quasistatic limit.[12,13] A system consisting of a line dipole sandwiched between two semi-infinite metal slabs [Fig. 1(a)] is transformed into two kissing nanowires illuminated by an incident plane wave [Fig. 1(b)]. In the transformed frame, the incoming beam is both absorbed and scattered by the nanostructure. We will show that the radiated field transforms into a fictive absorbing particle in the slab frame [see Fig. 1(a)]. Radiative losses correspond to the power dissipated by this small absorber. The radiative reaction is then considered to go beyond the electrostatic approximation. Taking into account the radiative reaction is necessary in order to satisfy the optical theorem (i.e., energy conservation).[17] In the transformed frame, it corresponds to the self-interaction between the particle and its own scattered field.[17–19] In the slab frame, we will show that the radiative reaction corresponds to the field scattered by the fictive absorbing particle and backemitted toward the metal slabs. This approach is general and can be applied to all the plasmonic devices that are derived using the conformal transformation approach.

In this paper, we first solve the problem in the slab geometry under the electrostatic approximation. Unlike previous works,[12,13] lossy surface waves (LSWs) (Refs. 20–22) are considered in addition to surface-plasmon polaritons (SPPs). Although LSWs and SPPs are in essence nonradiative in a metal slab geometry, they change in nature in the transformed frame. They propagate along the surface of a finite nanostructure [see Fig. 1(b)] and have a net dipole moment. This provides coupling with the incident field and gives rise to radiation losses. Taking into account LSWs is shown to

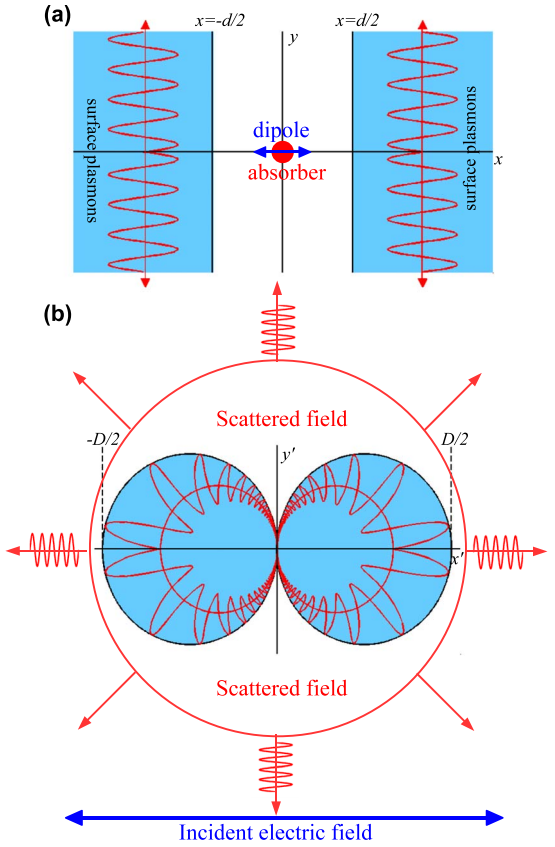

FIG. 1. (Color online) (a) Two semi-infinite metal slabs support SPPs that couple to a dipole source, transporting its energy to infinity. A fictive absorbing particle superimposed to the emitting dipole accounts for the radiative damping in the transformed geometry. (b) The transformed material consists of kissing cylinders. The dipole source $\mathbf{\Delta}$ is transformed into a uniform electric field $\mathbf{E_0'}$.

improve the analytical prediction of the absorption cross section around the surface-plasmon frequency ω_{sp}. Their consideration is also decisive to predict the scattering cross section in the quasistatic limit. Then, the radiative reaction is investigated to go beyond the electrostatic approximation. New analytical expressions of the scattering and absorption cross sections are derived and shown to be in a quantitative agreement with numerical simulations over a wide range of dimension (up to $D=200$ nm). Whereas the electrostatic result predicts an absorption cross-section scaling as D^2, our radiative model predicts a saturation of the absorption cross section around the physical cross section D. Interestingly, radiative losses are shown to improve the broadband performance of the device. Our analytical model would then allow to find the best compromise between the efficiency and the bandwidth of the light harvesting process, depending on which application is aimed at. The effect of radiative losses on the field enhancement induced by the nanostructure is also predicted. Whereas the electrostatic approximation predicts an electric field independent of the size of the device, radiative losses lead to a decrease in the field enhancement with the size of the nanostructure. Nevertheless, the device is shown to be quite robust to radiative damping since the maximum field enhancement remains superior to 10^3 over a major part of the near infrared and visible spectra for structure dimension $D<500$ nm.

II. SLAB GEOMETRY: TAKING INTO ACCOUNT LOSSY SURFACE WAVES

Our canonical system is a two-dimensional (2D) dipole that is contained in a thin slab of insulator of thickness d surrounded by two semi-infinite slabs of plasmonic material for $x<-d/2$ and $x>d/2$ [Fig. 1(a)]. Now apply the following conformal transformation:

$$z' = \frac{g^2}{z^*}, \tag{1}$$

where $z=x+iy$ and $z'=x'+iy'$ are the usual complex number notations. The superscript * stands for complex conjugate. g is an arbitrary constant. The resulting structure is a system of two kissing cylinders [Fig. 1(b)] of the same diameter,

$$\frac{D}{2} = \frac{2g^2}{d}. \tag{2}$$

The original dipole $\mathbf{\Delta}$, that we choose aligned along x, is transformed into a uniform electric field polarized along x',[12]

$$\mathbf{E_0'} = \frac{1}{2\pi\epsilon_o}\frac{\mathbf{\Delta}}{g^2}. \tag{3}$$

The conformal transformation is powerful since the optical response of kissing cylinders can be deduced by solving the tractable slab problem.

The near-field approximation is made, hence we assume that the Laplace's equation is obeyed. The coupling of the dipole with the two metallic sheets can be solved by expanding the incident field due to the dipole as a Fourier series in y. Applying the boundary conditions at each insulator/metal interface, the electrostatic potential induced by the two metal slabs in the insulator is given by[13]

$$\phi(|x|<d/2) = \frac{\mathbf{\Delta}}{2\pi\epsilon_o}\frac{\epsilon-1}{\epsilon+1}\int_{-\infty}^{+\infty}\frac{\sinh(|k|x)}{e^{|k|d}-\dfrac{\epsilon-1}{\epsilon+1}}e^{iky}dk. \tag{4}$$

As already pointed out in Ref. 13, the electric field induced by the metal slabs at the origin is of particular importance since it is directly related to the dipole moment of the kissing cylinders in the transformed frame. The electric field $\mathbf{E}(z=0)=-\nabla\phi|_{z=0}$ is given by

$$\mathbf{E}(z=0) = -\frac{\mathbf{\Delta}}{2\pi\epsilon_o}\frac{\epsilon-1}{\epsilon+1}\int_{-\infty}^{+\infty}\frac{|k|}{e^{|k|d}-\dfrac{\epsilon-1}{\epsilon+1}}dk. \tag{5}$$

To perform this integration, we write

$$|k| = \lim_{\delta\to 0}(k^2+\delta^2)^{1/2}.$$

The analytic structure of Eq. (5) is shown in Fig. 2. This integral is dominated by the pole close to the real axis for $\epsilon<-1$ which corresponds to SPPs carrying away energy to

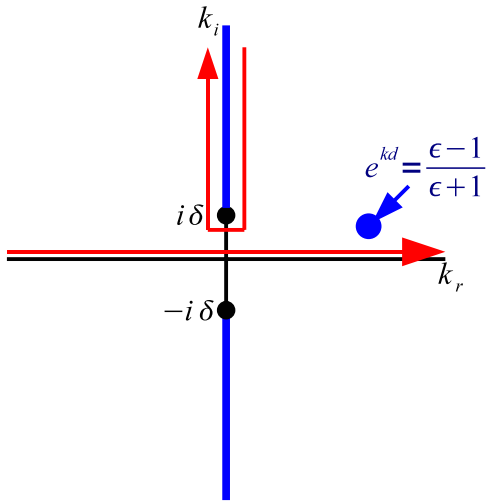

FIG. 2. (Color online) Analytic structure of the integrand of Eq. (5). There are two cuts running from $-i\delta$ and $+i\delta$ along the imaginary axis. There is also one pole if $\epsilon<-1$ (disk).

infinity. The cuts bring an additional contribution referred as LSWs or *creeping waves* in the literature.[20–22] These waves arise from the large wave vectors of the dipole and thus correspond to the response of the metal surface to the near field of the source. In previous works,[12,13] this contribution was neglected since SPPs are the major channel of energy dissipation below the surface-plasmon frequency in the configuration shown in Fig. 1(a). As will see in the following, the counterpart of LSWs in the transformed geometry also contributes to the net dipole moment of kissing nanowires. Hence, they give rise to radiation losses and their contribution to the scattering cross section is predominant in the low-frequency limit and above the surface-plasmon frequency.

If the LSWs are neglected, Eq. (5) can be computed, for $\epsilon<-1$, by picking out the pole due to SPPs,

$$\mathbf{E}^{\mathbf{sp}}(z=0) = -i\frac{\boldsymbol{\Delta}}{d^2\epsilon_o}\ln\left(\frac{\epsilon-1}{\epsilon+1}\right), \quad \text{if } \epsilon<-1, \tag{6}$$

where the superscript **sp** denotes the fact that only SPPs are taken into account. Note that, for $\epsilon>-1$, neglecting the LSWs leads to a zero electric field at $z=0$. On the contrary, if the contribution of the cuts in Fig. 2 is not neglected, it yields[23]

$$\mathbf{E}(z=0) = -\frac{\boldsymbol{\Delta}}{d^2\epsilon_o}\beta \tag{7}$$

with

$$\beta = \frac{1}{\pi}\frac{\epsilon-1}{\epsilon+1}\int_1^{+\infty} du \frac{\ln(u)}{u\left(u-\frac{\epsilon-1}{\epsilon+1}\right)} = \frac{1}{\pi}\mathrm{Li}_2\left(\frac{\epsilon-1}{\epsilon+1}\right), \tag{8}$$

where Li_2 is the dilogarithm function. A simpler analytical expression of β is not available. However, an approximation can be found for $\epsilon \ll -1$,

$$\beta \simeq \underbrace{i\ln\left(\frac{\epsilon-1}{\epsilon+1}\right)}_{\text{SPPs}} + \underbrace{\frac{\pi}{6} - \frac{2}{\epsilon+1}\left[1+\ln\left(-\frac{\epsilon+1}{2}\right)\right]}_{\text{LSWs}}. \tag{9}$$

This last expression highlights the respective contributions of SPPs and LSWs to the field reflected by the metal slabs at the origin. In the case of silver,[24] this approximation is valid in the range of frequency $\omega<0.95\omega_{sp}$.

The electric field induced at the dipole is of particular interest since it is directly related to the net dipole moment **p** of the kissing cylinders in the transformed geometry. Indeed, similarly to the relation linking the emitting dipole $\boldsymbol{\Delta}$ to a uniform electric field $\mathbf{E}_0'$ in the kissing cylinders geometry [Eq. (3)], the dipole moment **p** can be deduced from $\mathbf{E}(z=0)$,[13]

$$\mathbf{p} = 2\pi\epsilon_o g^2 \mathbf{E}(z=0). \tag{10}$$

Dipoles and fields exchange roles in the two frames but the product is unchanged. Therefore, energy dissipation is the same in each geometry. The power dissipated by the nanostructure in the transformed frame, P_{ext}, can be deduced from the slab problem[13]

$$P_{ext} = -\frac{\omega}{2}\mathrm{Im}\{\boldsymbol{\Delta}^* \cdot \mathbf{E}(z=0)\}. \tag{11}$$

If we inject the expressions of $\mathbf{E}(z=0)$ [Eq. (7)] and $\boldsymbol{\Delta}$ [Eq. (3)] into the last equation, replace d using Eq. (2), and renormalize it by the incoming flux $P_{in}=\epsilon_o c_o|\mathbf{E}_0'|^2/2$, the absorption cross section of the kissing cylinders can be deduced

$$\sigma_a^o = \frac{\pi^2}{4}k_o D^2\,\mathrm{Im}\{\beta\}, \tag{12}$$

where the superscript o stands for the electrostatic approximation. $k_o=\omega/c_o$ is the wave number in vacuum. Note that, rigorously, this expression corresponds to the extinction cross section of the kissing cylinders. However, as radiation losses are neglected under the quasistatic approximation, this quantity is here strictly equivalent to the absorption cross section.

Figure 3 displays the absorption spectra derived analytically with or without taking into account LSWs. The overall size is $D=20$ nm, such that the near-field approximation is valid. For this figure as well as in the following figures of the study, the metal is assumed to be silver with a surface-plasmon frequency $\omega_{sp}=3.67$ eV and permittivity taken from Johnson and Christy.[24] These analytical spectra are compared to the result of a numerical simulation, performed with the software COMSOL. Whereas the SPPs contribution is sufficient to describe the absorption cross section below ω_{sp}, considering LSWs is necessary for $\epsilon>-1$. There is a nice agreement between our analytical prediction and the numerical result. The comparison with the single cylinder case highlights the broadband feature of the kissing cylinders structure, as already widely discussed in Refs. 12 and 13.

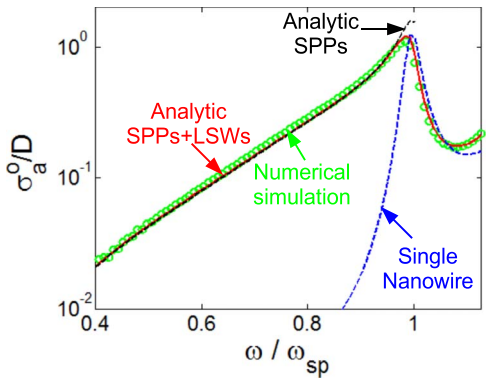

FIG. 3. (Color online) Absorption cross section σ_a^o normalized to the physical cross-section D as a function of frequency. The size of the device is $D=20$ nm. The results derived under the electrostatic approximation are thus considered. The analytical prediction with (red continuous line) or without (black dashed line) taking into account LSWs are compared to the result of a numerical simulation (green circles). The absorption spectrum of one single nanowire (blue dashed line) is also shown for comparison (Ref. 25–27).

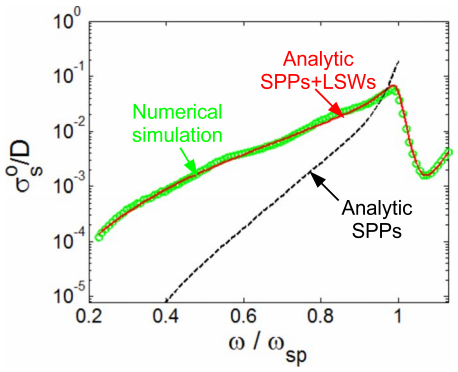

FIG. 4. (Color online) Scattering cross section σ_s^o normalized to the physical cross-section D as a function of frequency. The size of the device is $D=20$ nm. The results derived under the electrostatic approximation are thus considered. The analytical prediction with (red continuous line) or without (black dashed line) taking into account LSWs are compared to the result of a numerical simulation (green circles).

III. RADIATIVE LOSSES IN THE QUASISTATIC LIMIT

We now tackle with the scattering cross section of the nanostructure. In the transformed frame, the dyadic Green's function $\bar{\mathbf{G}}$ connects the electric dipole moment $\mathbf{p}$ at the origin $\mathbf{r}_\mathbf{0}'$ to the scattered electric field $\mathbf{E}_\mathbf{s}'$ at a position $\mathbf{r}'$,

$$\mathbf{E}_\mathbf{s}'(\mathbf{r}') = \bar{\mathbf{G}}(\mathbf{r}', \mathbf{r}_\mathbf{0}') \cdot \mathbf{p}. \tag{13}$$

The dyadic Green's function $\bar{\mathbf{G}}$ can be expressed as

$$\bar{\mathbf{G}}(\mathbf{r}', \mathbf{r}_\mathbf{0}') = (k_o^2 \bar{\mathbf{I}} + \nabla \cdot \nabla) G_o(\mathbf{r}', \mathbf{r}_\mathbf{0}'), \tag{14}$$

where $\bar{\mathbf{I}}$ is the unity dyad and $G_o(\mathbf{r}', \mathbf{r}_\mathbf{0}') = \mathcal{H}_o^{(1)}(k_o r)/(4i\epsilon_o)$ is the 2D scalar Green's function. Under the near-field approximation, the imaginary part of $\bar{G}$ can be simplified into

$$\mathrm{Im}\{\bar{\mathbf{G}}(|\mathbf{r}' - \mathbf{r}_\mathbf{0}'| \ll \lambda)\} = -i \frac{k_o^2}{8\epsilon_o} \bar{\mathbf{I}}. \tag{15}$$

Injecting this last equation into Eq. (13) leads to the following relation between the scattered field $\mathbf{E}_\mathbf{s}'$ and the dipole moment $\mathbf{p}$ in the near field,

$$\mathbf{E}_\mathbf{s}' = -i \frac{k_o^2}{8\epsilon_o} \mathbf{p}. \tag{16}$$

The kissing nanowires give rise to a uniform scattered field in the near field. Note that we have neglected the real part of the scattered field since it does not contribute to the radiation damping.

In the slab geometry, the uniform scattered field $\mathbf{E}_\mathbf{s}'$ is transformed into a dipole $\mathbf{\Delta}_\mathbf{s}$,

$$\mathbf{\Delta}_\mathbf{s} = 2\pi\epsilon_o g^2 \mathbf{E}_\mathbf{s}' = -i \frac{\pi}{4} g^2 k_o^2 \mathbf{p}. \tag{17}$$

Replacing $\mathbf{E}_\mathbf{s}'$ by Eq. (16) and $\mathbf{p}$ by Eq. (10) leads to

$$\mathbf{\Delta}_\mathbf{s} = -i \frac{\pi^2}{2} \epsilon_o g^4 k_o^2 \mathbf{E}(z=0). \tag{18}$$

This last expression indicates that the dipole $\mathbf{\Delta}_\mathbf{s}$ is directly proportional to $\mathbf{E}(z=0)$. Consequently, radiation losses in the transformed frame can be represented by an absorbing particle in the slab frame, of polarizability $\gamma_s = -i\pi^2 \epsilon_o g^4 k_o^2/2$.

The power P_s radiated by the kissing nanowires in the transformed frame is thus equivalent to the power absorbed by this fictive absorbing particle in the slab frame,

$$P_s = -\frac{\omega}{2} \mathrm{Im}\{\mathbf{\Delta}_\mathbf{s}^* \cdot \mathbf{E}(\mathbf{z}=\mathbf{0})\}. \tag{19}$$

If we inject the expressions of $\mathbf{E}(z=0)$ [Eq. (7)] and $\mathbf{\Delta}_\mathbf{s}$ [Eq. (18)] into the last equation, replace d using Eq. (2) and $\mathbf{\Delta}$ using Eq. (3), and finally renormalize P_s by the incoming flux $P_{in} = \epsilon_o c_o |\mathbf{E}_\mathbf{0}'|^2/2$, the scattering cross section of the kissing cylinders can be deduced in the quasistatic limit,

$$\sigma_s^o = \frac{\pi^4}{128} k_o^3 D^4 |\beta|^2. \tag{20}$$

Figure 4 displays σ_s^o as a fraction of the physical cross section, for $D=20$ nm. The analytic expression of σ_s^o is compared to the result of a numerical simulation, performed with the software COMSOL. An excellent agreement is found between numerical and theoretical results. Figure 4 also shows the predominance of LSWs for the radiative losses at low frequencies. If only SPPs are considered, the power radiated by the nanostructure is highly underestimated. Figure 4 shows that taking into account LSWs is essential to predict correctly the radiation losses.

IV. BEYOND THE ELECTROSTATIC APPROXIMATION: THE RADIATIVE REACTION

Figures 5 and 6 show the scattering and absorption cross sections provided by numerical simulations for different size

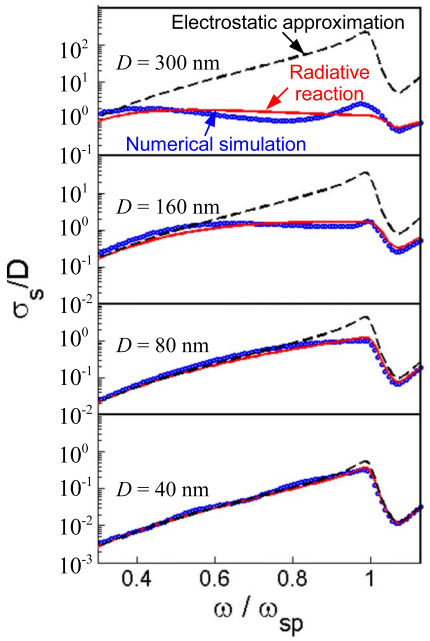

FIG. 5. (Color online) Scattering cross section normalized to the physical cross section as a function of frequency for different size D=40, 80, 160, 300 nm (from bottom to top). The analytical prediction σ_s taking into account the radiative reaction [Eq. (24), red continuous line] is compared to the quasistatic limit σ_s^o [Eq. (20), black dashed line] and to the result of a numerical simulation (blue circles).

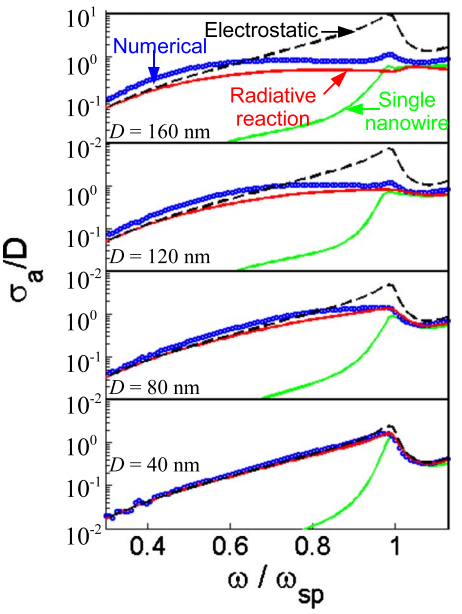

FIG. 6. (Color online) Absorption cross section normalized to the physical cross section as a function of frequency for different size D=40, 80, 120, 160 nm (from bottom to top). The analytical prediction σ_a taking into account the radiative reaction [Eq. (25), red continuous line] is compared to the quasistatic limit σ_a^o [Eq. (12), black dashed line] and to the result of a numerical simulation (blue dots). The absorption spectrum of one single nanowire is also shown for comparison in green (Ref. 25).

D. These numerical spectra are compared to the analytical expression of the scattering and absorption cross sections derived in the quasistatic limit [Eqs. (12)–(20)]. Clearly, the electrostatic approximation is no longer checked for dimension $D>40$ nm. The aim of this section is to show how we can go beyond this approximation and derive analytical expressions of the absorption and scattering cross sections taking into account the radiation damping.

In the literature, several studies have shown how the optical response of nanostructures can be predicted analytically beyond the electrostatic approximation by taking into account the radiative reaction.[17–19] It accounts for the self-interaction between the scattered field $\mathbf{E}_s'$ and the induced dipole moment $\mathbf{p}$ itself. In the slab geometry, the radiative reaction corresponds then to the interaction between the fictive small absorber $\mathbf{\Delta_s}$ and the induced electric field $\mathbf{E}(z=0)$. It can be easily derived in the slab geometry, adding the contribution of the absorbing dipole $\mathbf{\Delta_s}$ to the expression of the induced electric field $\mathbf{E}(z=0)$ in Eq. (7),

$$\mathbf{E}(z=0) = -\frac{\mathbf{\Delta}+\mathbf{\Delta_s}}{d^2\epsilon_o}\beta. \tag{21}$$

Replacing $\mathbf{\Delta_s}$ by its expression [Eq. (18)] allows to derive a new expression of $\mathbf{E}(z=0)$ in presence of radiative losses,

$$\mathbf{E}(z=0) = -\frac{\mathbf{\Delta}}{d^2\epsilon_o}\frac{\beta}{1-i\pi^2\beta g^4 k_o^2/(2d^2)}. \tag{22}$$

If we inject this new expression of $\mathbf{E}(z=0)$ into Eq. (11) and replace d and $\mathbf{\Delta}$ using Eqs. (2) and (3), respectively, a new expression of the extinction cross section can be found,

$$\sigma_{ext} = \frac{\pi^2}{4}k_o D^2\,\mathrm{Im}\left\{\frac{\beta}{1-i\pi^2 k_o^2 D^2\beta/32}\right\}. \tag{23}$$

Similarly, a new expression of the radiated power can be derived by injecting the new expression of $\mathbf{E}(z=0)$ [Eq. (22)] into Eq. (19). Then, by renormalizing P_s by the incoming flux P_{in}, a new expression for the scattering cross section can be found

$$\sigma_s = \frac{\pi^4}{128}k_o^3 D^4\frac{|\beta|^2}{|1-i\pi^2 k_o^2 D^2\beta/32|^2}. \tag{24}$$

The radiative correction appears at the denominator of the last equation. This analytical expression of σ_s is compared to numerical simulations and quasistatic predictions for different size of nanostructures in Fig. 5. The result is spectacular: whereas the electrostatic prediction clearly overestimates the numerical result, Eq. (24) predicts quantitatively the scattering cross section of kissing cylinders for $40<D<200$ nm. For larger size (see the top graph in Fig. 5), the agreement between theory and numerical simulations becomes qualitative but our model still provides a satisfying order of magnitude for the scattering cross section. The comparison of σ_s^o and σ_s in Fig. 5 highlights the effect of the radiative reaction which tends to smooth the radiative spectrum. The scattering cross section clearly saturates at the level of the physical cross section.

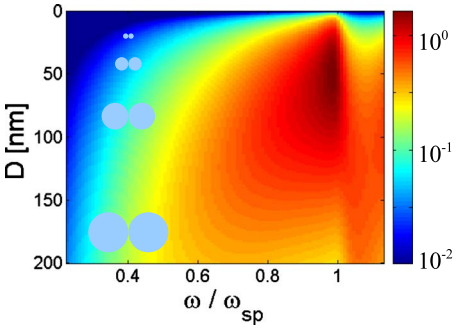

FIG. 7. (Color online) Absorption cross-section σ_a [Eq. (25)] normalized to the physical cross section as a function of frequency and the size D of the system. The color bar is in log scale.

Knowing σ_s [Eq. (24)] and σ_{ext} [Eq. (23)], a new expression for the absorption cross section is also deduced using $\sigma_a = \sigma_{ext} - \sigma_s$,

$$\sigma_a = \frac{\pi^2}{4} k_o D^2 \frac{\mathrm{Im}\{\beta\}}{|1 - i\pi^2 k_o^2 D^2 \beta/32|^2}. \tag{25}$$

The same radiative correction as for σ_s [Eq. (24)] appears at the denominator of the last equation. This analytical expression of σ_a is compared to numerical simulations and quasistatic predictions for different size of nanostructures in Fig. 6. For $D < 200$ nm, a good agreement is found between our analytical calculations and numerical simulations, although our theoretical model underestimates slightly the numerical result. The numerical spectrum is also slightly red shifted compared to the theoretical prediction. This is due to the retardation effects which are not taken into account. The comparison with electrostatic results points out the beneficial effect of considering the radiative reaction. Figure 6 also displays the absorption cross section obtained for a single cylinder of dimension D. The comparison with the single cylinder case highlights the gain in terms of broadband spectrum provided by the dimer.

Figure 7 displays our analytical calculation of the absorption cross section σ_a as a function of frequency and the structure dimension D. Radiation losses improve the broadband performance of the device by shifting the absorption spectrum toward red when the structure dimension increases. Nevertheless, they also make the absorption cross-section fall compared to the physical cross section. The information provided by Fig. 7 might be very useful in the perspective of experiments. Depending on the aimed application, an optimized dimension for the structure can be found. If a large broadband spectrum is required, then a structure of size $D = 130$ nm is ideal. On the contrary, if an efficient light harvesting is wanted, then a dimension of 50 nm may provide an absorption cross section larger than the kissing cylinders physical cross section over a smaller bandwidth.

V. FIELD ENHANCEMENT BEYOND THE ELECTROSTATIC APPROXIMATION

In previous works,[12,13] the kissing cylinders nanostructure was shown to exhibit drastic nanofocusing properties. Figure 8 shows the electric field along the surface of the kissing cylinders for $\omega = 0.9\omega_{sp}$, plotted as a function of the angle θ defined in the inset. Under the electrostatic approximation, the electric field is independent of the size of the device. It can be extremely high, exceeding 10^4 over a major part of the visible and near-infrared spectra. However, the electrostatic result is valid typically for devices smaller than 20 nm. Radiation damping breaks the independence of the electric field relative to the structure dimension, making the field enhancement decrease for larger structure dimensions. This fact is illustrated by Fig. 8(a) which compares the electrostatic results with the field enhancement obtained numerically for a structure dimension of 100 nm. Whereas the electrostatic theory predicts a field enhancement of 2×10^3, the numerical result shows a maximum field enhancement of 10^3. The aim of this section is to predict analytically the effect of radiation losses on the field enhancement and predict the nanofocusing performance as a function of the structure dimension.

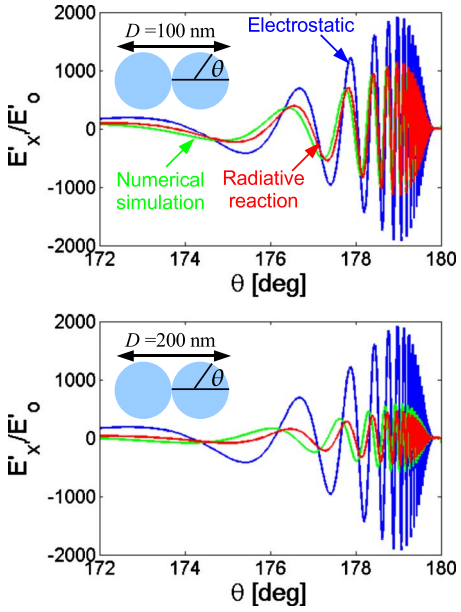

FIG. 8. (Color online) Electric field along the x' polarization normalized by the incident electric field E_0' shown at the surface of one kissing nanowire as a function of the angle θ defined in the inset, for (a) $D = 100$ nm and (b) $D = 200$ nm. The frequency is $\omega = 0.9\omega_{sp}$. The analytical prediction with the radiative reaction (red) is compared to the numerical result (green) and to the electrostatic one (blue).

To derive the effect of radiative losses on the field enhancement, let us come back first into the slab frame. Comparing the expressions of $\mathbf{E}(z=0)$ derived under and beyond the electrostatic approximation [Eqs. (7) and (22)], the presence of an absorber accounting for radiative losses leads to renormalizing the emitting dipole $\mathbf{\Delta}$ by a factor,

$$\eta = 1 - i\pi^2 \beta g^4 k_o^2/(2d^2). \tag{26}$$

The same correction can be made in the transformed frame. Radiative reaction leads to renormalizing the electric field derived under the electrostatic approximation in Ref. 13 by

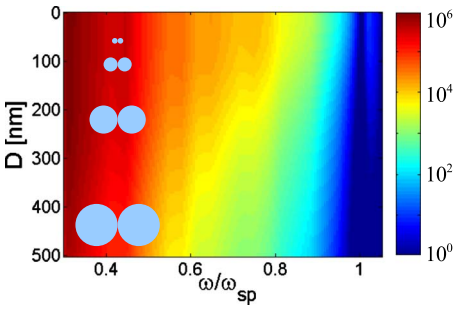

FIG. 9. (Color online) Maximum field enhancement E'_{max}/E'_0 [Eq. (28)] as a function of frequency and the size D of the kissing nanowires. The color bar is in log scale.

the same factor η. Using Eq. (2), this factor η can be expressed as a function of D,

$$\eta = 1 - i\frac{\pi^2}{32}k_o^2 D^2 \beta. \tag{27}$$

Figure 8 shows the result of this renormalization. The electric field derived under the electrostatic approximation has been normalized by the factor η. There is a nice agreement with the numerical result for $D=100$ and 200 nm. This shows how our analytical model can provide an accurate estimation of the field enhancement for large plasmonic structures. The correction is quite simple since it consists in a simple renormalization of the electrostatic result by the factor η. However, it does not predict the slight change in phase shown by the numerical simulation when the structure dimension increases. This change in phase comes from the retardation effects which are not considered in our model.

In our previous work, the maximum field enhancement that can be expected along the cylinders surface has been derived analytically [Eq. 43 in Ref. 13]. Normalizing this analytical expression by the absolute value of the factor η [Eq. (27)], one can obtain the maximum field enhancement that can be expected in presence of radiation damping,

$$\left|\frac{E'_{max}}{E'_0}\right| \simeq \frac{2\pi}{e^2}\frac{\left|\ln\left(\frac{\epsilon-1}{\epsilon+1}\right)\sqrt{\frac{\epsilon^2+1}{\epsilon^2-1}}\right|}{|1-i\pi^2 k_o^2 D^2\beta/32|}\frac{(|\epsilon|^2-1)^2}{\epsilon_I^2}, \tag{28}$$

where ϵ_I is the imaginary part of the permittivity. Figure 9 displays the maximum field enhancement that may induce kissing nanowires as a function of frequency and of the structure dimension. The low-size limit ($D<20$ nm) corresponds to the electrostatic result. The frequency dependence of the field enhancement in this regime has already been discussed in Ref. 13: the dissipation losses increase when we approach the surface plasmon frequency and tend to truncate the growth of the electric field along the kissing nanowires surface. Figure 9 shows how radiation losses affect the field enhancement. The latter one decreases regularly with the structure dimension. However, as pointed out previously with the absorption cross section, the kissing nanowires are quite robust to radiation losses: even for dimension of 500 nm, the field enhancement induced by the structure remains significant ($>10^3$) over a major part of the near-infrared and visible spectra ($\omega<0.8\omega_{sp}$). The result displayed by Fig. 9 is important in perspective of experiments: even if the structure dimension is comparable with the wavelength, kissing nanowires can provide a drastic nanofocusing of light. Moreover, for such a dimension, nonlocal and quantum-mechanical effects[26,27] would have less influence than for kissing nanowires of a few tens of nanometers. The field enhancement predicted here for $D>100$ nm is then more realistic than the one derived for smaller nanostructures.[12,13]

VI. CONCLUSION

In this paper, the conformal transformation theory applied to plasmonics has been extended beyond the quasistatic limit. We have shown that radiation damping can be represented by a fictive small absorbing particle in the original (slab) geometry. Lossy surface waves (as well as the surface-plasmon mode) have a net dipole moment in the transformed geometry and contribute predominantly to radiative losses in the low-frequency limit. Analytical expressions for the scattering and absorption cross sections of the nanostructure have been derived beyond the quasistatic limit, taking into account the radiative reaction. A comparison with numerical simulations has shown that our model allows to predict quantitatively the optical response of nanostructures for $D<200$ nm. Radiative losses make the absorption cross-section fall compared to the physical cross section of the system. Thus, they limit the light-harvesting capabilities of the device but improve its broadband properties. Similarly, the radiative reaction leads to a renormalization of the electric field derived under the electrostatic approximation. Despite radiation damping, the field enhancement induced by the structure remains significant ($\sim 10^3$), especially at low frequencies ($\omega<0.8\omega_{sp}$). Throughout this study, we have considered the example of kissing nanowires, but our approach can be applied to all the nanostructures derived with the conformal transformation approach. These results open nice perspectives since this study extends the range of dimension over which the plasmonic system will perform an efficient light harvesting and drastic nanofocusing of its energy. Larger structures will be easier to manufacture and less sensitive to quantum-mechanical or nonlocal effects, which are likely to limit the nanofocusing performance of the device at the nanoscale.

ACKNOWLEDGMENTS

The authors wish to thank Yu Luo for fruitful discussions. This work was supported by the European Community project PHOME (Contract No. 213390) and by the U.K. Engineering and Physical Sciences Research Council (EPSRC).

[1] U. Leonhardt, Science **312**, 1777 (2006).
[2] J. B. Pendry, D. Schurig, and D. R. Smith, Science **312**, 1780 (2006).
[3] D. Schurig, J. J. Mock, B. Justice, S. A. Cummer, J. B. Pendry, A. F. Starr, and D. R. Smith, Science **314**, 977 (2006).
[4] J. Li and J. B. Pendry, Phys. Rev. Lett. **101**, 203901 (2008).
[5] R. Liu, C. Ji, J. J. Mock, J. Y. Chin, T. J. Cui, and D. R. Smith, Science **323**, 366 (2009).
[6] J. Valentine, J. Li, T. Zentgraf, G. Bartal, and X. Zhang, Nature Mater. **8**, 568 (2009).
[7] L. H. Gabrielli, J. Cardenas, C. B. Pointras, and M. Lipson, Nat. Photonics **3**, 461 (2009).
[8] T. Ergin, N. Stenger, P. Brenner, J. B. Pendry, and M. Wegener, Science **328**, 337 (2010).
[9] P. A. Huidobro, M. L. Nesterov, L. Martin-Moreno, and F. J. García-Vidal, Nano Lett. **10**, 1985 (2010).
[10] Y. Liu, T. Zentgraf, G. Bartal, and X. Zhang, Nano Lett. **10**, 1991 (2010).
[11] J. Renger, M. Kadic, G. Dupont, S. S. Aćimović, S. Guenneau, R. Quidant, and S. Enoch, Opt. Express **18**, 15757 (2010).
[12] A. Aubry, D. Y. Lei, A. I. Fernández-Domínguez, Y. Sonnefraud, S. A. Maier, and J. B. Pendry, Nano Lett. **10**, 2574 (2010).
[13] D. Y. Lei, A. Aubry, S. A. Maier, and J. B. Pendry, New J. Phys. **12**, 093030 (2010).
[14] A. Aubry, D. Y. Lei, S. A. Maier, and J. B. Pendry, Phys. Rev. B **82**, 125430 (2010).
[15] Y. Luo, J. B. Pendry, and A. Aubry, Nano Lett. **10**, 4186 (2010).
[16] J. B. Pendry, Opt. Express **11**, 755 (2003).
[17] B. T. Draine, Astrophys. J. **333**, 848 (1988).
[18] A. Wokaun, J. P. Gordon, and P. F. Liao, Phys. Rev. Lett. **48**, 957 (1982).
[19] R. Carminati, J.-J. Greffet, C. Henkel, and J. M. Vigoureux, Opt. Commun. **261**, 368 (2006).
[20] G. W. Ford and W. H. Weber, Phys. Rep. **113**, 195 (1984).
[21] W. L. Barnes, J. Mod. Opt. **45**, 661 (1998).
[22] P. Lalanne and J. P. Hugonin, Nat. Phys. **2**, 551 (2006).
[23] R. C. McPhedran and W. T. Perrins, Appl. Phys. (Berlin) **24**, 311 (1981).
[24] P. B. Johnson and R. W. Christy, Phys. Rev. B **6**, 4370 (1972).
[25] C. H. Bohren and D. R. Huffman, *Absorption and Scattering of Light by Small Particles* (Wiley, New York, 1983).
[26] J. Zuloaga, E. Prodan, and P. Nordlander, Nano Lett. **9**, 887 (2009).
[27] F. J. García de Abajo, J. Phys. Chem. C **112**, 17983 (2008).